Lower limits for the homogenization of periodic metamaterials made from electric dipolar scatterers

Ramakrishna Venkitakrishnan,[1,*] Timon Höß,[1] Taavi Repän,[2] Fatima Z. Goffi,[3] Michael Plum,[3] and Carsten Rockstuhl[1,2]

[1]*Institute of Theoretical Solid State Physics, Wolfgang-Gaede-Straße 1, Karlsruhe Institute of Technology, 76131 Karlsruhe, Germany*

[2]*Institute of Nanotechnology, Karlsruhe Institute of Technology, P.O. Box 3640, 76021 Karlsruhe, Germany*

[3]*Institute for Analysis, Karlsruhe Institute of Technology, Englerstraße 2, 76131 Karlsruhe, Germany*

(Received 22 February 2021; revised 19 April 2021; accepted 21 April 2021; published 20 May 2021)

Nonlocal constitutive relations promise to homogenize metamaterials even though the ratio of period over operational wavelength is not much smaller than unity. However, this ability has not yet been verified, as frequently only discrete structures were considered. This denies a systematic variation of the relevant ratio. Here, we explore, using the example of an electric dipolar lattice, the superiority of the nonlocal over local constitutive relation to homogenize metamaterials when the period tends to be comparable to the wavelength. Moreover, we observe a breakdown of the ability to homogenize the metamaterial at shorter lattice constants. This surprising failure occurs when energy is transported across the lattice thanks to a well-pronounced near-field interaction among the particles forming the lattice. Contrary to common wisdom, this suggests that the period should not just be much smaller than the operational wavelength to homogenize a metamaterial, but, for a given size of the inclusion, there is an optimal period.

DOI: 10.1103/PhysRevB.103.195425

Optical metamaterials are artificial media made from subwavelength unit cells that can control the propagation of light in a way inaccessible with natural materials [1,2]. The existence of inductive and capacitive elements within the unit cell results in strong resonances. Numerous applications such as a "perfect lens" to achieve imaging with subwavelength resolution [3], the reduction of the total scattering cross section for transparency and cloaking [4–6], the enhancement of the magnetic flux density at a desired location for wireless power transfer [7–9], and many more [10,11] have been suggested and realized based on metamaterials.

The two-dimensional (2D) equivalent of metamaterials, called metasurfaces, are composed of periodically arranged electrically small scatters on a 2D lattice [12–15]. Metasurfaces are capable to alter the amplitude, phase, and polarization of the incoming electromagnetic wave in a disruptive sense. In comparison with its three-dimensional counterpart, metasurfaces provide reduced loss and ease of fabrication, thus being a promising candidate for planar optical devices [16–19].

In discussing the optical action of metamaterials and to consider them in the design of applications, it is more convenient to consider them as a homogeneous medium rather than a granular material made from discrete scatterers [20]. The establishment of a link between these two representations of the same material is called homogenization and is at the heart of a theoretical description of metamaterials [21,22].

For natural materials made from a discrete arrangement of atoms or molecules separated by a characteristic length a, supposed to be much smaller than the relevant wavelength λ_0 (i.e., $ak_0 = a\frac{2\pi}{\lambda_0} \lll 1$), the electromagnetic response at the effective level is obtained from the average of the local electromagnetic fields across a mesoscopic volume [23]. This volume has to be large to contain many constituents, but it has to be sufficiently small with respect to the wavelength as well.

Such averaging leads to local constitutive relations. There, the induced response at some specific point in space, e.g., expressed in terms of an electric displacement or a magnetic field, depends only on the electric field or the magnetic induction at the very same spatial location.

This description has been carried over to artificial photonic materials [24]. It is noteworthy that field averaging is a fundamental technique and henceforth has facilitated in deriving further advanced and accurate numerical retrieval models [25–28]. However, these techniques usually assume that the critical length scale continues to be small compared to the relevant wavelength. But the constituents in such artificial photonic materials are already more mesoscopic in size and typically characterized by a spatial extent that is smaller, but not much smaller any longer, than the relevant wavelength ($ak_0 < 1$).

But this mesoscopic nature made it possible to observe a strong magnetic response in these artificial photonic materials. In essence, as all materials from which metamaterials are made are intrinsically nonmagnetic, it requires a finite spatial extent of the unit cells so that a variation of the electric field across the unit cells can induce ring-type currents [29,30]. This gives rise to an artificial, i.e., an induced, magnetic response at the effective level. The appearance of the magnetic response is called weak spatial dispersion (WSD) because the gradient of the electric field matters in this description. After a suitable gauge transformation, the response can be expressed with local constitutive relations where the electric response is expressed via a permittivity and the magnetic response via a permeability [31]. However, when considering metamaterials

*Corresponding author: ramakrishna.venkitakrishnan@kit.edu

with a characteristic length a comparable to the wavelength λ_0, it can be shown that local constitutive relations fail to predict the electromagnetic properties [2,32]. To make that point clear: we expect a single set of material parameters to explain reflection and transmission from a thin film of the material independent of the angle of incidence. If we would have to consider a different material property at each angle, the introduction of effective properties would be meaningless. Unfortunately, for many mesoscopic metamaterials, this is exactly the case and it turns out that local constitutive relations are insufficient [31].

To overcome this limitation, alternative first-principles and self-consistent homogenization theories have been proposed [33,34], introducing a dispersive behavior for the material response with respect to the spatial coordinates [35–39]. Here, we rely on the approach described in [40,41], where nonlocal constitutive relations have been suggested that capture effects due to a strong spatial dispersion (SSD). These constitutive relations express the response in terms of the local electric fields, its first- and second-order derivatives, and a larger number of higher-order gradients [42]. In the systematic derivation of such constitutive relations, the point of departure is the nonlocal response function $\hat{R}(\mathbf{r}-\mathbf{r}', k_0)$ at the effective level. The nonlocal response function is supposed to describe the metamaterial in the most accurate sense. In spatial Fourier space, such constitutive relation reads

$$\mathbf{D}(\mathbf{k}, k_0) = \hat{\tilde{R}}(\mathbf{k}, k_0)\mathbf{E}(\mathbf{k}, k_0), \tag{1}$$

where k_0 is the free space wave number corresponding to the frequency, $\mathbf{k}$ is the wave vector of the plane wave solution, and $\mathbf{D}(\mathbf{k}, k_0)$ and $\mathbf{E}(\mathbf{k}, k_0)$ are the electric displacement and the electric field, respectively.

To have a practically usable form for the constitutive relation, we require that the spatial dispersion must vanish at long wavelengths, $|\mathbf{k}| \to 0$, and approximate the kernel by a Taylor polynomial,

$$\begin{aligned} D_i(\mathbf{k}, k_0) = (\delta_{ij} + a_{ij})E_j + b_{ijk}k_kE_j + c_{ijkl}k_kk_lE_j \\ + d_{ijklm}k_kk_lk_mE_j + e_{ijklmn}k_kk_lk_mk_nE_j. \end{aligned} \tag{2}$$

In a real space description, after inverse Fourier transform, the terms where some wave vector components are multiplied with the electric field convert to gradients of the electric field. To exploit this ansatz, not all of these terms in the expansion shall be considered. The number of terms after which the series is truncated offers a handle to establish the constitutive relations of increasing complexity. In our contribution, we investigate two constitutive relations to homogenize a material made from isotropic electric dipole scatterers on a square lattice with lattice constant a. This geometry has inversion symmetry. It does not support magnetoelectric coupling effects. Thereby, only even-order terms survive in the Taylor series expansion of this constitutive relation. A truncation of the series after the second order and after the fourth order, and by requiring specific forms for the Taylor coefficients in terms of curl operators [40,43], leads to the following two constitutive relations that we consider:

$$\mathbf{D}(\mathbf{k}, k_0) = \epsilon(k_0)\mathbf{E}(\mathbf{k}, k_0) - \mathbf{k} \times (\alpha(k_0)\mathbf{k}\times)\mathbf{E}(\mathbf{k}, k_0) \tag{3}$$

and

$$\begin{aligned} \mathbf{D}(\mathbf{k}, k_0) = \epsilon(k_0)\mathbf{E}(\mathbf{k}, k_0) - \mathbf{k} \times (\alpha(k_0)\mathbf{k}\times)\mathbf{E}(\mathbf{k}, k_0) \\ + \mathbf{k} \times \mathbf{k} \times (\gamma(k_0)\mathbf{k}\times)\mathbf{k} \times \mathbf{E}(\mathbf{k}, k_0). \end{aligned} \tag{4}$$

Equation (3) is referred to as the weak spatial dispersion (WSD). The two material parameters characterizing the model are the electric permittivity $\epsilon(k_0)$ and the second-order term $\alpha(k_0)$. Equation (4) is referred to as the strong spatial dispersion model (SSD) or the nonlocal model, which additionally includes the nonlocal parameter $\gamma(k_0)$ as an effective parameter.

Upon considering the nonuniqueness nature of the displacement field $\mathbf{D}(\mathbf{k}, k_0)$, a suitable gauge field can translate the second-order material parameter $\alpha(k_0)$ into an effective magnetic permeability $\mu(k_0)$ as $\alpha = (k_0^2\mu)^{-1}(\mu - 1)$. This translates the second-order response of the homogeneous material to an artificial local magnetic response. Therefore, this second-order term and an artificial magnetism are synonymous.

While the superiority of the nonlocal constitutive relation has already been proven, so far only selected examples have been considered [43,44]. A systematic quantification of the improvement depending on the typical length scale relative to the wavelength has not been possible. With exact structures such as the fishnet metamaterial or even simpler metamaterials such as spheres on a cubical lattice, such analysis is not that easy because a change in the geometry usually changes the entire optical response of the unit cell. It is important to mention that the homogeneous models considered here can be applied to any mesoscopic centrosymmetric slab structures, irrespective of the shape of the scatterer [45–47].

Therefore, it is the purpose of our contribution to resort to the potentially most simple metamaterial and to investigate the possibility to homogenize it with local and nonlocal constitutive relations. This simplest structure is a square array of electric dipoles that is driven into resonance at some characteristic frequency [48,49]. The typical length scale is the periodicity a. It will be shown that for larger periods a description with SSD is systematically superior and can also cope very well with scenarios where the size of the period tends to be comparable to the wavelength.

As an extension, we also report an unexpected finding. While common wisdom suggests that the smaller the period, the better the structure can be homogenized, we show that this does not hold. Indeed, for very small periods, both constitutive relations tend to capture the effective response less accurately, even though the SSD model is always better. This surprising finding can be explained by the spread of excitation across the array for tightly packed arrangements thanks to a heavily pronounced near-field coupling among the particles. Such breakdown of a homogenization at very small periods is unexpected and points towards the existence of a range of mesoscopic periods most optimal for an effective description. On a technical level, we employ the T-matrix method [50] that is based on Mie theory [51,52] to simulate from the actual structure for reference reflection and transmission. This method is particularly suitable as we can consider a generic representation of an electric dipolar scatterer with exact moments giving high-quality numerical approximations

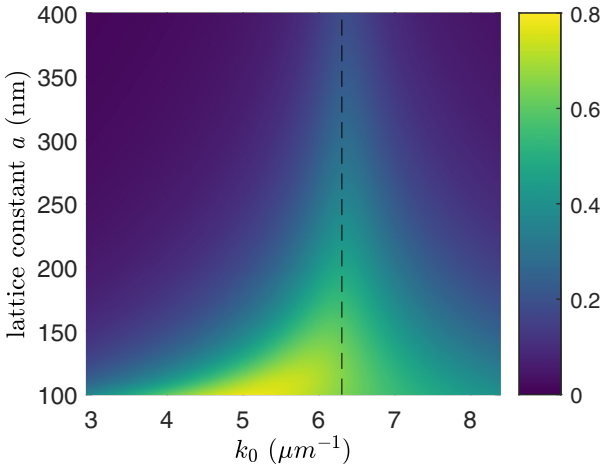

FIG. 1. Amplitude of the reflection coefficient, $|\rho^{\mathrm{REF}}(k_0, k_x = 0)|$, for a range of lattice constants generated using the general Mie method.

[53]. We always assume the electric dipolar particles to have a resonance at $k_{0_{\mathrm{iso}}} = 6.3\ \mu\mathrm{m}^{-1}$. Its Lorentzian dispersion is characterized by an Ohmic loss of $0.1k_{0_{\mathrm{iso}}}c_0$ and an oscillator strength of $6\ \sqrt{2}\pi c_0$, which results in a full width at half maximum of about 50 nm. Here, c_0 represents the speed of light in vacuum.

In the homogenization, we then need to identify the homogeneous material characterized by its respective material parameters that can explain these numerically simulated optical coefficients in an optimal sense [54–57]. For that purpose, we first solve for the dispersion relation and the eigenmodes sustained in a medium characterized by the constitutive relation given in Eqs. (3) and (4) with a plane wave ansatz. The medium made from the periodically arranged electric dipolar scatterers is considered as a slab with a finite thickness that corresponds to the considered periodicity. That leaves us with a high-symmetry unit cell where the effective properties are isotropic. We consider a linearly polarized plane wave as the illumination and, upon enforcing the interface conditions [58], we can analytically calculate the complex reflection and transmission coefficients for the homogeneous medium [40]. Afterwards, we perform a dedicated fitting procedure to identify the material parameters that fit the optical coefficients obtained from the homogeneous slab in an optimal sense to the optical coefficients obtained in the full wave optical simulations.

As a selected example for the outcome of the full wave simulations, Fig. 1 shows the absolute value of ρ^{REF} as a function of the frequency (k_0) at normal incidence ($k_x = 0$) for a range of lattice constants a. It can be clearly seen that for large lattice constants, the reflection spectra follow the polarizability of the particle. A reflection peak can be seen at the resonance frequency assumed for the particles (dashed line) at $k_{0_{\mathrm{iso}}} = 6.3\ \mu\mathrm{m}^{-1}$. The resonance width follows the line width. Decreasing the lattice periods in lowest-order approximation only increases the amplitude of the reflection thanks to the higher filling fraction. On decreasing a further, the resonance redshifts relative to the isolated particle resonance. The ability of the considered homogenization models to capture this feature is a way to qualitatively judge the considered models.

The retrieval of the effective properties is done at each frequency independently. It exploits the angular-dependent optical coefficients from a slab in some selected polarization. First, these optical coefficients, i.e., reflection $\rho^{\mathrm{model}}(k_0, k_x; \epsilon, \mu, \gamma)$ and transmission $\tau^{\mathrm{model}}(k_0, k_x; \epsilon, \mu, \gamma)$, are computed for a given set of material parameters. In the case of WSD, only ϵ and μ are considered, while in the case of SSD, ϵ, μ, and γ are considered. The deviation of the reference values and those obtained from the homogenous model are expressed as

$$f^{\rho} = \rho^{\mathrm{REF}}(k_0, k_x) - \rho^{\mathrm{model}}(k_0, k_x; \epsilon, \mu, \gamma),$$
$$f^{\tau} = \tau^{\mathrm{REF}}(k_0, k_x) - \tau^{\mathrm{model}}(k_0, k_x; \epsilon, \mu, \gamma),$$

with model = {WSD,SSD}. The goodness of the fit at each frequency is judged using an objective function $\delta(k_0)$ defined as

$$\delta(k_0) = \min_{\epsilon,\mu,\gamma} \frac{\sum_{k_x=0}^{k_0} \omega(k_0, k_x)(|f^{\rho}|^2 + (|f^{\tau}|^2)}{\sum_{k_x=0}^{k_0} \omega(k_0, k_x)}, \tag{5}$$

where $\omega(k_0, k_x)$ represents a weight function which is introduced to ensure a good fit at least in the paraxial regime and to stretch the trend towards higher angles of incidence. We have chosen $\omega(k_0, k_x)$ to be the Fermi-Dirac function,

$$\omega(k_0, k_x) = \left[1 + \exp\left(\frac{\frac{k_x}{k_0} - u}{v}\right)\right]^{-1}, \tag{6}$$

where u and v are the auxiliary variables to adjust the position and smoothness of ω, chosen to be 0.66 and 0.05, respectively. In the actual fitting procedure, the material parameters at a given frequency are adjusted until a minimum for $\delta(k_0)$ has been found.

We exploit in the retrieval the Transverse Magnetic (TM)-k_x illumination with the principle propagation direction k_z. The transverse wave vector is calculated as $k_x = k_0 \sin(\theta)$. As incident angles, we considered $\theta : [0^\circ, 90^\circ)$ divided into 100 values. The calculations are done for 240 frequencies in the range $k_0 = [3, 8.4]\ \mu\mathrm{m}^{-1}$. The considered lattice constant lies in the space $a = [100, 400]$ nm. For the longest period and the highest frequency considered, we are in a regime where the period is approximately half the free space wavelength. With this parameter range, the homogenization models are brought close to the regime where the system is clearly mesoscopic. A first diffraction order continues to be absent, but the system is expected to support strong spatial dispersion effects [31].

To appreciate the improvement offered by the SSD model, we begin by investigating the considered array using the WSD model. After having retrieved the effective properties, Fig. 2 shows the recalculated $|\rho|$ with these material parameters as a function of k_0 and a at normal incidence. This figure shows the ability of the local model to capture the resonant features as seen in the reference Fig. 1. Figure 3 shows the effective material parameter for the pertinent sample homogenized with the WSD model.

Notice in Fig. 3 that the permeability $\mu(k_0)$ acquires a secondary resonance at frequencies larger than $k_{0_{\mathrm{iso}}}$. On reducing the lattice constants, this secondary resonance further exhibits

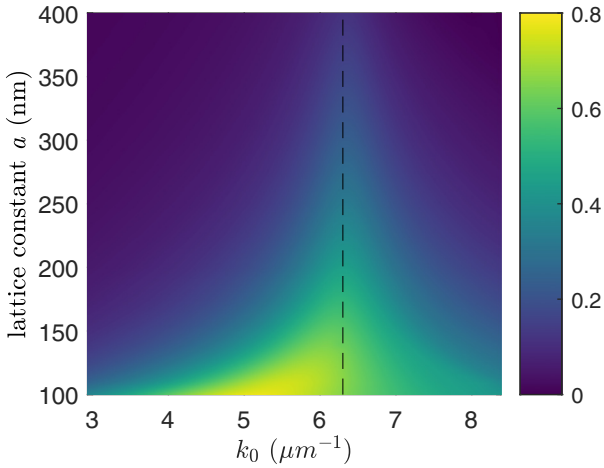

FIG. 2. Amplitude value of the reflection coefficient $|\rho|$ retrieved using the WSD model for comparison with the data.

a blueshift. The physical origin of this secondary resonance is the excitation of an antisymmetric mode in the lattice, where the dipole moments in adjacent particles oscillate π out of phase. To reveal this more clearly, Fig. 4 shows $|\rho^{\mathrm{REF}}|$ at three different incidence angles: $\theta = 0^\circ, 30^\circ$, and 60°. Figure 4(a) shows the redshift in the resonant frequency from $k_{0_{\mathrm{iso}}}$ at normal incidence. This can be attributed to the in-phase oscillation of the adjacent dipoles corresponding to the symmetric mode of the coupled oscillator. The apparent redshift is expected from ordinary hybridization theory [59,60]. On the other hand, Figs. 4(b) and 4(c) show a developing secondary resonance corresponding to the out-of-phase oscillation of the adjacent dipoles as in the antisymmetric mode. Such an antisymmetric mode corresponds to a fraction of a ring current. Therefore, it is no surprise that it emerges in the effective permeability.

This collective oscillation of electric dipoles in the array at lower lattice constants can be understood as a characteristic

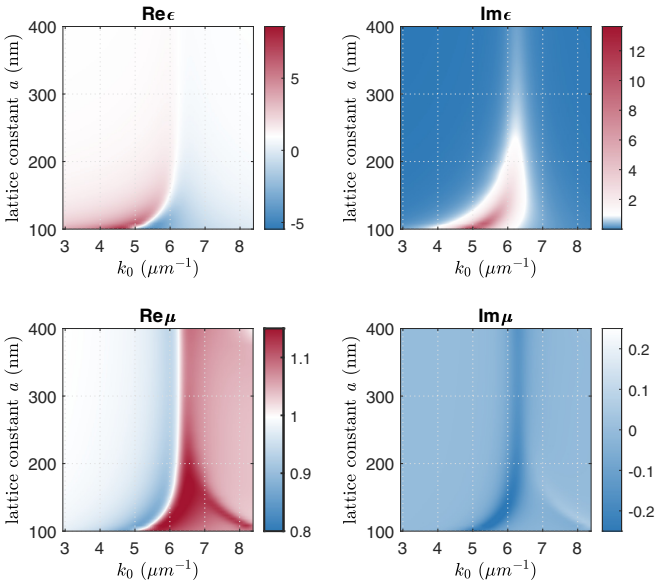

FIG. 3. Effective material parameter, permittivity $\epsilon(k_0)$ and permeability $\mu(k_0)$, retrieved with the WSD model.

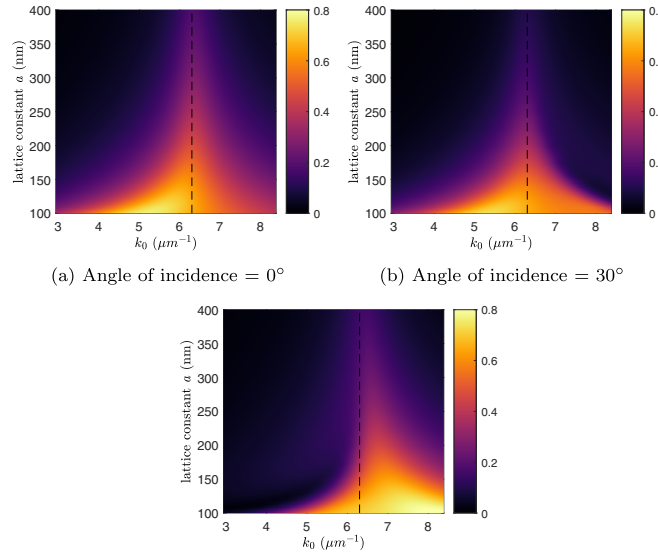

(a) Angle of incidence = 0° (b) Angle of incidence = 30°

(c) Angle of incidence = 60°

FIG. 4. Amplitude of the reflection coefficient $|\rho^{\mathrm{REF}}|$ as calculated with the general Mie method at different angles of incidence. (a) The value at normal incidence of light; here, only the symmetric oscillation of the dipole is visible. (b),(c) The value at angles 30° and 60°, respectively, showing the growth of secondary resonance on increasing the angle of incidence.

feature of the strong spatial dispersion. A local constitutive relation is not able to capture it, but it is expected to be accounted for by the nonlocal parameter. This constitutes the motivation to investigate the SSD model at the considered parameter range.

The fitting procedures for the nonlocal constitutive relation, given by Eq. (4), are carried out as a 6D optimization problem using the aforementioned objective function and the same weight function.

The fitting procedure shall ensure that the material parameters are a continuous function of k_0. While no special care was required for the WSD case, this continuity is not trivial for the SSD model. The practical problem is the appearance of two branches of solutions that are distinguished by the sign of $\mathrm{Im}\gamma(k_0)$. A clear distinction of the two branches is possible by performing the retrieval with a restricted parameter space to either $\mathrm{Im}\gamma < 0$ or $\mathrm{Im}\gamma > 0$. The global optimum corresponds to one of these branches in different frequency regions, as can be seen from Fig. 5. The figure shows $\delta(k_0)$ for the two possible branches. A notable difference appears for frequencies above $k_0 \approx 5.1\ \mu\mathrm{m}^{-1}$. One of the branches seems to be preferred in spectral proximity to the resonance, while the other branch seems to be preferred at short wavelengths. To judge the necessary sign, we investigated the energy flux in such media that has to point away from the source. Based on that consideration, which is discussed in the Appendix, it can be concluded that the solution with $\mathrm{Im}\gamma > 0$ is the right solution. It will be considered from now on.

To discuss the improvement in our ability to describe the pertinent material at the homogenous level, Fig. 6 shows the objective function $\delta(k_0)$ in a logarithmic scale as a function of the lattice constant for both models. Across the considered frequency space, the SSD model provides a better fit

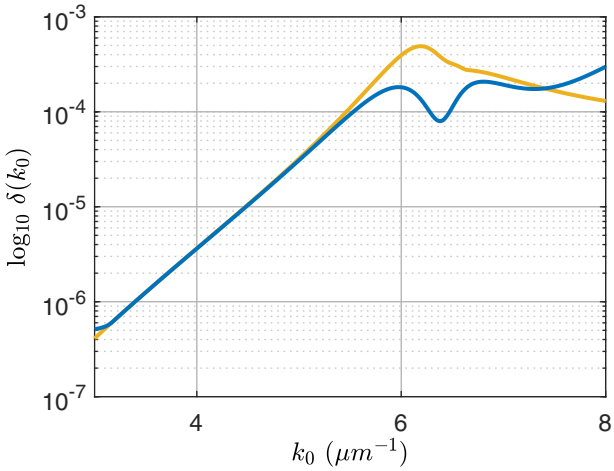

FIG. 5. Branching solution of the objective function $\delta(k_0)$ for the electric dipole array with a fixed lattice constant $a = 250$ nm. The curve splits into two different branches at $k_0 = 5.1\ \mu\text{m}^{-1}$ with the blue curve for $\text{Im}\gamma(k_0) < 0$ and the yellow curve for $\text{Im}\gamma(k_0) > 0$.

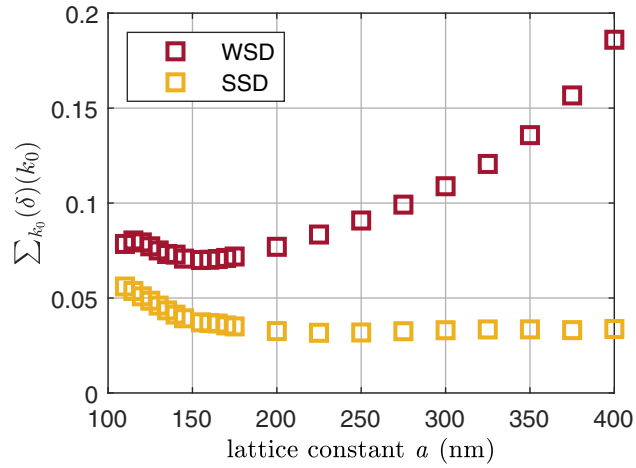

FIG. 7. Sum of objective function over the considered frequency range plotted against the respective lattice constant. The red squares denote the WSD model and the yellow squares denote the SSD model.

with the reference data when describing the medium at the effective level. The improvement of the fit is significant by at least one order of magnitude, especially near the resonance $k_{0_{\text{iso}}}$. Further, towards the antisymmetric resonance frequency, using the nonlocal constitutive relation gives an appreciable improvement up to one order of magnitude. This suggests that the considered nonlocal material properties from Eq. (4) can be used to reliably predict the optical response from the slab in a situation that deviates from those that have been considered in the general (local) properties of the materials.

To lift the comparison and the assessment of the two methods to a higher level, we plot in Fig. 7 the sum of the objective function over the frequency space, $\sum_{k_0}\delta(k_0)$, as a function of lattice constants. Many things can be seen from that figure.

First, the SSD model is always superior when compared to the WSD model to describe the material at an effective level. The objective function is always lower by at least a factor of two; and, in some frequency regions, the improvement corresponds to an order of magnitude. This improvement is attributed to the nonlocal parameter $\gamma(k_0)$ that accounts for the corrections in the local parameters. This clearly underpins

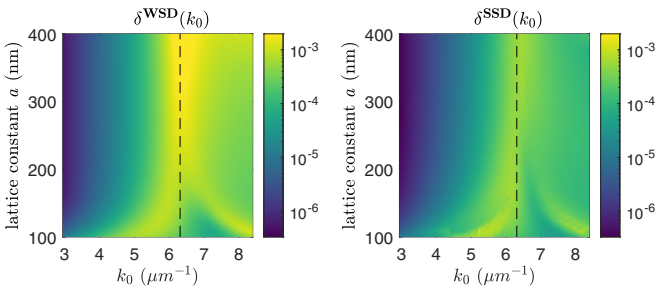

(a) $\delta^{\text{WSD}}(k_0)$ (b) $\delta^{\text{SSD}}(k_0)$

FIG. 6. The objective function $\delta(k_0)$ in logarithmic scale as a function of frequency in the considered range of lattice constants. (a) The WSD model. (b) The SSD model. In comparison, the SSD model has a better fit compared to the WSD model.

the necessity of the fourth-order term in the effective description of the electric dipole array.

Second, the improvement is particularly convincing for large periods, i.e., when effects due to spatial dispersion are expected to be most pronounced. Here, the SSD model is able to homogenize the material in good approximation, even independent of the period.

Third, when decreasing the period, the improvement is less pronounced and both models tend to explain the response better. This makes perfect sense because the homogenization is expected to be more reliable when the period tends to be (much) smaller compared to the operational wavelength.

However, there is a fourth aspect that is somewhat surprising. This plot suggests a critical value for the lattice constant, $a_{\text{critical}} = 200$ nm, below which the ability to homogenize the material deteriorates. While the SSD model continues to be more reliable, the frequency averaged deviation increases with smaller lattice constants. These values of a fall within the parametric range where the antisymmetric modes are excited, and so the secondary resonance is not fully accounted by the effective parameters in the SSD model. The inability to describe such materials with local constitutive relations can be explained by the spread of an excitation across the material by means of a near-field interaction. The individually polarized particle can transport its energy across larger distances within the material by coupling to its nearest neighbors. Indeed, such coupling mechanism was considered to be responsible as a wave guiding mechanism [61,62] and it is such mechanism that prohibits the homogenization of the material with a local constitutive relation, i.e., the WSD model. But, also, a next-higher-order nonlocal material model, i.e., the SSD model, has problems in capturing these effects. This limits the applicability of the considered models to give the effective full description of the slab for lower lattice constants, and thus a_{critical} can be considered as the lower limit for the homogenization for the electric dipole slab. The observation of such a lower limit in the particle spacing for the homogenization of materials is notable.

As a short conclusion, we have been studying the ability to homogenize an array of electric dipoles using a local and a nonlocal constitutive relation. It was shown that the nonlocal constitutive relation can capture the effects of a strong spatial dispersion that are expected to appear for large periods much better. In essence, we have not observed a notable degradation in the ability of the model to homogenize the metamaterial in this regime. For the largest period, the nonlocal constitutive relation was roughly better by one order of magnitude. When the period got smaller, the superiority of the nonlocal constitutive relation became less pronounced, as expected, but continued to be better by at least a factor of two. Besides these somewhat expected results, we also observed, somewhat surprisingly, that for very small periods, both constitutive relations tend to capture the optical response less optimally. These phenomena occur because for a very dense packaging of scatterers, an excitation can also spread across the lattice, thanks to a pronounced near-field interaction among adjacent particles. This spread of excitation can be quite far reaching, which denies, in essence, any homogenization. Therefore, this hints towards an optimal period at which a homogenization of the lattice is possible. This insight can be safely expected to shape our understanding of how to homogenize metamaterials.

ACKNOWLEDGMENTS

The authors gratefully acknowledge financial support by the Deutsche Forschungsgemeinschaft (DFG, German Research Foundation) through Project-ID No. 258734477 - SFB 1173 and through Project-ID No. 390761711 - EXC 2082/1.

APPENDIX

In this Appendix, we shall summarize the more standardized Poynting vector approach towards judging the right sign for the imaginary component of the parameter γ. Poynting vector $\langle S\rangle$ corresponding to the energy flux in the homogeneous medium is derived for the SSD model. For each case, the sign associated with $\langle S\rangle$ is studied.

Considering the relevant constitutive relation $\mathbf{D}(\mathbf{k}, k_0) = \hat{\hat{R}}(\mathbf{k}, k_0)\mathbf{E}(\mathbf{k}, k_0)$ with TM polarization, the Ampere's law reads

$$\begin{pmatrix} 0 & -k_z & k_y \\ k_z & 0 & -k_x \\ -k_y & k_x & 0 \end{pmatrix} \mathbf{H}(\mathbf{k}, k_0) + k_0 \hat{R}(\mathbf{k}, k_0)\mathbf{E}(\mathbf{k}, k_0) = 0, \tag{A1}$$

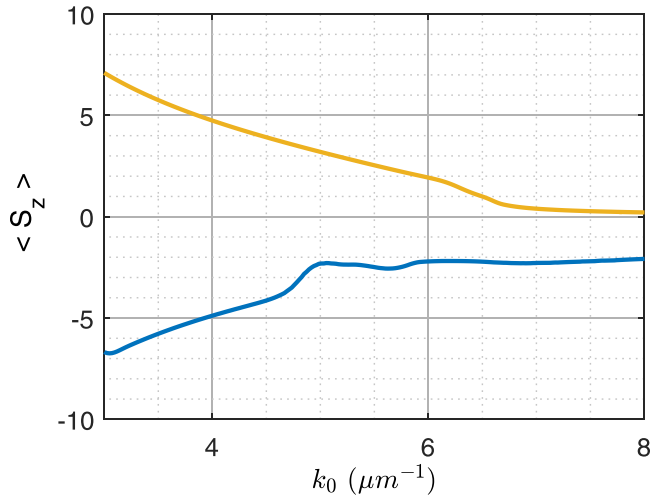

FIG. 8. Poynting vector $\langle S_z\rangle$ for the electric dipole array with a fixed lattice constant $a = 250$ nm. Here, the blue curve refers to $\mathrm{Im}\gamma(k_0) < 0$ and the yellow curve refers to $\mathrm{Im}\gamma(k_0) > 0$. The curve denoting $\mathrm{Im}\gamma(k_0) > 0$ shows the energy flux to be in the direction away from the source $[(\langle S_z\rangle) > 0]$, which is the right solution.

and its H_y solution can be written as

$$H_y(\mathbf{k}, k_0) = E_x(\mathbf{k}, k_0)\frac{\left[k_0^2\mu_y p_0 + \left(k_x^2\epsilon_x + k_z^2\epsilon_z\right)(\mu_y - 1)\right]}{k_z k_0 \mu_y \epsilon_z}, \tag{A2}$$

where

$$p_0 = k_x^4\gamma_z\epsilon_x + k_z^4\gamma_x\epsilon_z + k_x^2k_z^2(\gamma_x\epsilon_x + \gamma_z\epsilon_z) + \epsilon_x\epsilon_z.$$

So the time average energy flux for the considered SSD model is

$$\langle S_z\rangle = \mathrm{Re}(\mathbf{S_z}) = E_x^2\frac{\left[k_0^2\mu_y p_0 + \left(k_x^2\epsilon_x + k_z^2\epsilon_z\right)(\mu_y - 1)\right]}{k_z k_0 \mu_y \epsilon_z}. \tag{A3}$$

To discuss the derived quantity numerically, an electric dipole array with a fixed lattice $a = 250$ nm is chosen. Equation (A3) is employed to calculate the energy flux for both choices of $\mathrm{Im}\gamma > 0$. Figure 8 shows the time averaged energy flux corresponding to the relevant eigenmode (the k_z value corresponding to the new mode from the SSD). It can be concluded that the flux associated with $\mathrm{Im}\gamma > 0$ flow away from the source and hence is the right solution.

[1] T. J. Cui, D. R. Smith, and R. Liu, *Metamaterials* (Springer, New York, 2010).
[2] F. Capolino, *Theory and Phenomena of Metamaterials* (CRC Press, Boca Raton, FL, 2017).
[3] J. B. Pendry, Negative Refraction Makes a Perfect Lens, Phys. Rev. Lett. **85**, 3966 (2000).
[4] M. G. Silveirinha, A. Alù, and N. Engheta, Parallel-plate metamaterials for cloaking structures, Phys. Rev. E **75**, 036603 (2007).
[5] S. A. Tretyakov, A personal view on the origins and developments of the metamaterial concept, J. Opt. **19**, 013002 (2016).
[6] R. Fleury, F. Monticone, and A. Alu, Invisibility and Cloaking: Origins, Present, and Future Perspectives, Phys. Rev. Appl. **4**, 037001 (2015).
[7] M. Song, P. Smirnov, E. Puhtina, E. Zanganeh, S. Glybovski, P. Belov, and P. Kapitanova, Multi-mode metamaterial-inspired resonator for near-field wireless power transfer, Appl. Phys. Lett. **117**, 083501 (2020).

[8] M. Song, P. Belov, and P. Kapitanova, Wireless power transfer inspired by the modern trends in electromagnetics, Appl. Phys. Rev. **4**, 021102 (2017).

[9] A. Alù, F. Bilotti, N. Engheta, and L. Vegni, Theory and simulations of a conformal omni-directional subwavelength metamaterial leaky-wave antenna, IEEE Trans. Antennas Propag. **55**, 1698 (2007).

[10] A. Poddubny, I. Iorsh, P. Belov, and Y. Kivshar, Hyperbolic metamaterials, Nat. Photon. **7**, 948 (2013).

[11] F. Capolino, *Applications of Metamaterials* (CRC Press, Boca Raton, FL, 2017).

[12] P. Genevet and F. Capasso, Holographic optical metasurfaces: A review of current progress, Rep. Prog. Phys. **78**, 024401 (2015).

[13] S. M. Kamali, E. Arbabi, A. Arbabi, and A. Faraon, A review of dielectric optical metasurfaces for wavefront control, Nanophotonics **7**, 1041 (2018).

[14] C. Zou, J. Sautter, F. Setzpfandt, and I. Staude, Resonant dielectric metasurfaces: Active tuning and nonlinear effects, J. Phys. D **52**, 373002 (2019).

[15] A. Rahimzadegan, D. Arslan, R. N. S. Suryadharma, S. Fasold, M. Falkner, T. Pertsch, I. Staude, and C. Rockstuhl, Disorder-Induced Phase Transitions in the Transmission of Dielectric Metasurfaces, Phys. Rev. Lett. **122**, 015702 (2019).

[16] J. Bohn, T. Bucher, K. E. Chong, A. Komar, D.-Y. Choi, D. N. Neshev, Y. S. Kivshar, T. Pertsch, and I. Staude, Active tuning of spontaneous emission by Mie-resonant dielectric metasurfaces, Nano Lett. **18**, 3461 (2018).

[17] A. K. Iyer, A. Alù, and A. Epstein, Metamaterials and metasurfaces historical context, recent advances, and future directions, IEEE Trans. Antennas Propag. **68**, 1223 (2020).

[18] N. K. Gupta, H. Wanare, and S. A. Ramakrishna, Design of transparent conducting plasmonic metasurfaces and theory of impedance-matched metastructures, Plasmonics **15**, 2109 (2020).

[19] D. Arslan, S. Fasold, A. Rahimzadegan, T. Kawde, S. Linss, N. Abbasirad, M. Falkner, M. Decker, C. Rockstuhl, T. Pertsch *et al.*, Tailored structural disorder in optical metasurfaces, in *2018 Conference on Lasers and Electro-Optics Pacific Rim (CLEO-PR)* (IEEE, Hong Kong, China, 2018), pp. 1–2.

[20] M. Kadic, G. W. Milton, M. van Hecke, and M. Wegener, 3D metamaterials, Nat. Rev. Phys. **1**, 198 (2019).

[21] C. R. Simovski, On electromagnetic characterization and homogenization of nanostructured metamaterials, J. Opt. **13**, 013001 (2010).

[22] I. Tsukerman, A. N. M. S. Hossain, and Y. D. Chong, Homogenization of layered media: Intrinsic and extrinsic symmetry breaking, Europhys. Lett. **133**, 17003 (2021).

[23] V. M. Agranovich and V. Ginzburg, *Crystal Optics with Spatial Dispersion, and Excitons*, Vol. 42 (Springer Science & Business Media, New York, 2013).

[24] D. R. Smith and J. B. Pendry, Homogenization of metamaterials by field averaging, JOSA B **23**, 391 (2006).

[25] A. Andryieuski, S. Ha, A. A. Sukhorukov, Y. S. Kivshar, and A. V. Lavrinenko, Bloch-mode analysis for retrieving effective parameters of metamaterials, Phys. Rev. B **86**, 035127 (2012).

[26] C. R. Simovski, Bloch material parameters of magneto-dielectric metamaterials and the concept of Bloch lattices, Metamaterials **1**, 62 (2007).

[27] D. R. Smith, Analytic expressions for the constitutive parameters of magnetoelectric metamaterials, Phys. Rev. E **81**, 036605 (2010).

[28] A. Andryieuski, C. Menzel, C. Rockstuhl, R. Malureanu, F. Lederer, and A. Lavrinenko, Homogenization of resonant chiral metamaterials, Phys. Rev. B **82**, 235107 (2010).

[29] J. Zhou, T. Koschny, M. Kafesaki, E. N. Economou, J. B. Pendry, and C. M. Soukoulis, Saturation of the Magnetic Response of Split-Ring Resonators at Optical Frequencies, Phys. Rev. Lett. **95**, 223902 (2005).

[30] B. Lahiri, S. G. McMeekin, A. Z. Khokhar, R. M. D. L. Rue, and N. P. Johnson, Magnetic response of split ring resonators (srrs) at visible frequencies, Opt. Express **18**, 3210 (2010).

[31] C. Menzel, T. Paul, C. Rockstuhl, T. Pertsch, S. Tretyakov, and F. Lederer, Validity of effective material parameters for optical fishnet metamaterials, Phys. Rev. B **81**, 035320 (2010).

[32] C. R. Simovski and S. A. Tretyakov, Local constitutive parameters of metamaterials from an effective-medium perspective, Phys. Rev. B **75**, 195111 (2007).

[33] S. Lannebère, T. A. Morgado, and M. G. Silveirinha, First principles homogenization of periodic metamaterials and application to wire media, Comptes Rendus. Phys. **21**, 367 (2020).

[34] J. V. Alvarez, B. Djafari-Rouhani, and D. Torrent, Generalized elastodynamic model for nanophotonics, Phys. Rev. B **102**, 115308 (2020).

[35] P. Kinsler, An introduction to spatial dispersion: Revisiting the basic concepts, Photon. Nanostructures Fundam. Appl. **43**, 100897 (2021).

[36] A. Shevchenko, P. Grahn, V. Kivijärvi, M. Nyman, and M. Kaivola, Spatially dispersive functional optical metamaterials, J. Nanophoton. **9**, 093097 (2015).

[37] D. Torrent, Strong spatial dispersion in time-modulated dielectric media, Phys. Rev. B **102**, 214202 (2020).

[38] D. Iakushev and S. Lopez-Aguayo, Nonlocal effect on transverse-magnetic photonic properties of periodic dielectric-metal stacks, J. Opt. **20**, 105101 (2018).

[39] T. Karamanos, T. Zygiridis, and N. Kantartzis, Homogenization of 3D metamaterial particle arrays for oblique propagation via a point-dipole analysis, Eur. Phys. J. Appl. Phys. **91**, 20902 (2020).

[40] K. Mnasri, A. Khrabustovskyi, C. Stohrer, M. Plum, and C. Rockstuhl, Beyond local effective material properties for metamaterials, Phys. Rev. B **97**, 075439 (2018).

[41] F. Z. Goffi, K. Mnasri, M. Plum, C. Rockstuhl, and A. Khrabustovskyi, Towards more general constitutive relations for metamaterials: A checklist for consistent formulations, Phys. Rev. B **101**, 195411 (2020).

[42] F. Z. Goffi, A. Khrabustovskyi, R. Venkitakrishnan, C. Rockstuhl, and M. Plum, Higher order constitutive relations and interface conditions for metamaterials with strong spatial dispersion, (unpublished).

[43] K. Mnasri, A. Khrabustovskyi, M. Plum, and C. Rockstuhl, Retrieving effective material parameters of metamaterials characterized by nonlocal constitutive relations, Phys. Rev. B **99**, 035442 (2019).

[44] K. Mnasri, F. Z. Goffi, M. Plum, and C. Rockstuhl, Homogenization of wire media with a general purpose nonlocal constitutive relation, J. Opt. Soc. Am. B **36**, F99 (2019).

[45] T. Takeuchi and K. Yabana, Extremely large third-order nonlinear optical effects caused by electron transport in quantum plasmonic metasurfaces with subnanometer gaps, Sci. Rep. **10**, 21270 (2020).

[46] M. Mattheakis, C. A. Valagiannopoulos, and E. Kaxiras, Epsilon-near-zero behavior from plasmonic Dirac point: Theory and realization using two-dimensional materials, Phys. Rev. B **94**, 201404(R) (2016).

[47] T. Liu, R. Xu, P. Yu, Z. Wang, and J. Takahara, Multipole and multimode engineering in mie resonance-based metastructures, Nanophotonics **9**, 1115 (2020).

[48] M. Goodarzi and T. Pakizeh, Retrieving effective surface susceptibilities of high-index metasurfaces based on dipole approximation, Opt. Commun. **483**, 126659 (2021).

[49] S. A. Tretyakov, On the homogenization of dense planar arrays of scatterers, Electromagnetics **19**, 201 (1999).

[50] D. Beutel, A. Groner, T. Höß, C. Rockstuhl, and I. Fernandez-Corbaton, Efficient simulation of bi-periodic, layered structures with the t-matrix method, in *2020 Fourteenth International Congress on Artificial Materials for Novel Wave Phenomena (Metamaterials)* (IEEE, New York, 2020), pp. 110–112.

[51] G. Mie, Beiträge zur optik trüber medien, speziell kolloidaler metallösungen, Ann. Phys. **330**, 377 (1908).

[52] T. Wriedt, Mie theory: A review, *The Mie Theory* (Springer, New York, 2012), pp. 53–71.

[53] A. Rahimzadegan, R. Alaee, C. Rockstuhl, and R. W. Boyd, Minimalist Mie coefficient model, Opt. Express **28**, 16511 (2020).

[54] C. A. Valagiannopoulos, On measuring the permittivity tensor of an anisotropic material from the transmission coefficients, Prog. Electromagn. Res. **9**, 105 (2008).

[55] C. Valagiannopoulos, Predicting the quantum texture from transmission probabilities, J. Appl. Phys. **127**, 174301 (2020).

[56] X. Han, Z. Fan, Z. Liu, C. Li, and L. J. Guo, Inverse design of metasurface optical filters using deep neural network with high degrees of freedom, InfoMat **3**, 432 (2021).

[57] R. Pestourie, C. Pérez-Arancibia, Z. Lin, W. Shin, F. Capasso, and S. G. Johnson, Inverse design of large-area metasurfaces, Opt. Express **26**, 33732 (2018).

[58] A. Khrabustovskyi, K. Mnasri, M. Plum, C. Stohrer, and C. Rockstuhl, Interface conditions for a metamaterial with strong spatial dispersion, arXiv:1710.03676.

[59] E. Prodan and P. Nordlander, Plasmon hybridization in spherical nanoparticles, J. Chem. Phys. **120**, 5444 (2004).

[60] P. Nordlander, C. Oubre, E. Prodan, K. Li, and M. I. Stockman, Plasmon hybridization in nanoparticle dimers, Nano Lett. **4**, 899 (2004).

[61] M. Quinten, A. Leitner, J. R. Krenn, and F. R. Aussenegg, Electromagnetic energy transport via linear chains of silver nanoparticles, Opt. Lett. **23**, 1331 (1998).

[62] S. A. Maier, M. L. Brongersma, P. G. Kik, and H. A. Atwater, Observation of near-field coupling in metal nanoparticle chains using far-field polarization spectroscopy, Phys. Rev. B **65**, 193408 (2002).